Sapphirine-Bearing Pelitic Granulite from Ailaoshan Orogen, West Yunnan, China: Metamorphic Conditions and Tectonic Setting

Cheng Wei[1,2], **Yuhao Zhao**[3], **Luhua Zhu**[4], **Xuexiang Qi**[*1], **Zhihui Cai**[1], **Xufeng Liu**[1], **Guangfei Ma**[5]

1. *Key Laboratory for Continental Dynamics of Ministry of Land and Resources, Institute of Geology, Chinese Academy of Geological Sciences, Beijing 100037, China*
2. *School of Earth and Space Sciences, Peking University, Beijing 100871, China*
3. *Nanjing Institute of Geology and Mineral Resources, Chinese Academy of Geological Sciences, Nanjing 210016, China*
4. *Geology Bureau for Nonferrous Metals of Guangdong Province, Guangzhou 510080, China*
5. *Hangzhou Mechanical Design Research Institute of Ministry of Water Resources, Standard & Quality Control Research Institute of Ministry of Water Resources, Hangzhou 310012, China*

Cheng Wei: https://orcid.org/0000-0001-9432-5663; Xuexiang Qi: https://orcid.org/0000-0002-1570-8189

ABSTRACT: To reveal the petrological characteristics, metamorphic evolution history and tectonic setting of the pelitic granulites from Ailaoshan Orogen, West Yunnan, China, a comprehensive study in mineral chemistry, petrogeochemistry and geochronology studies is presented in this paper. Two metamorphic stages of the granulites can be established: (1) the peak metamorphism recorded by the mineral assemblage of garnet, kyanite, K-feldspar and rutile, and the initial retrograde metamorphism shown by the mineral assemblage of garnet, sillimanite, sapphirine, spinel, K-feldspar, plagioclase and biotite; (2) the superimposed metamorphism recorded by the mineral assemblage of biotite, muscovite, plagioclase, quartz and ilmenite. Zircon LA-ICP-MS U-Pb dating indicates that the protolith of the granulite was deposited after 337 Ma. The initial retrograde metamorphism occurred at *P-T* conditions of 8.6–12 kbar at 850–920 ºC estimated by mineral assemblages, the low pressure limit of kyanite stability and GBPQ geothermobarometer in Indosinian (about 235 Ma), and the late superimposed metamorphism occurred at the *P-T* condition of 3.5–3.9 kbar at 572–576 ºC estimated by GBPQ geothermobarometer since 33 Ma. The first stage was related to the amalgamation of the South China and Indochina blocks during the Triassic, and the second stage was possibly related with the large scale sinistral slip-shearing since the Oligocene. It is inferred that the upper continental crust was subducted/underthrusted to the lower continental crust (deeper than 30 km) and underwent granulite-facies metamorphism and then quickly exhumed to the middle-upper crust (10–12 km) and initial retrograde metamorphism occurred due to the collision of the Indochina and South China blocks during Indosinian, which was followed by superimposition of the second stage of metamorphism since the Oligocene.

KEY WORDS: high-pressure pelitic granulite, sapphirine, zircon, LA-ICP-MS, U-Pb, dating, metamorphic rocks, Ailaoshan Orogen.

0 INTRODUCTION

High-pressure pelitic granulite is characterized by the key associated kyanite-K-feldspar in felsic bulk composition (O'Brien and Rötzler, 2003), and is a result of continental collision and amalgamation leading to the significant burial and crustal thickening (Zhang et al., 2018, 2000; Anderson et al., 2012; Jöns and Schenk, 2011; Santosh et al., 2009; Brown, 2007; Zhang and Meng, 2005; O'Brien and Rötzler, 2003; Gilotti and Elvevold, 2002; Schaller et al., 1999; Hiroi et al., 1994). It is an important indicator to define the past block convergence boundary and understand the history of a tectonic zone.

Ailaoshan-Jinshajiang tectonic zone, located at the northeastern margin of the Indochina Block (Fig. 1a), was formed by subduction and collision between the Indochina and South China blocks in Permo–Triassic (Wang B D et al., 2018; Qi et al., 2016; Jian et al., 2009; Yumul et al., 2008; Owada et al., 2007; Trung et al., 2006; Lepvrier et al., 2004; Liu et al., 2000; Wang X F et al., 2000; Mo et al., 1993; Sengör, 1984), followed by the southeastward extrusion of the Indochina Block and strike slip-shearing overprinted on the sutures during the northward subduction of the India Plate in the Cenozoic (Liu et al., 2007; Morley, 2007; Zhang et al., 2006, 1999; Burchfiel and Wang, 2003; Wang et al., 2001; Leloup et al., 1995; Leloup and Kienast, 1993; Tapponnier
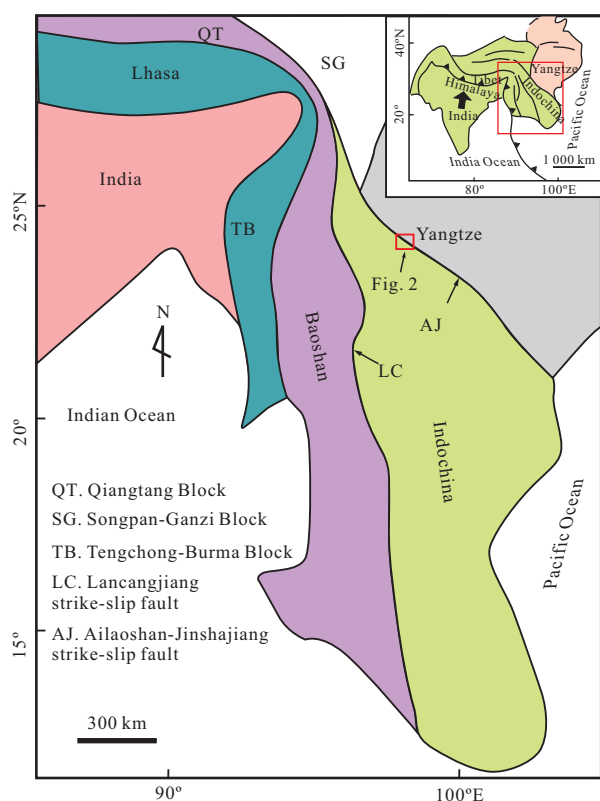

Figure 1. Simplified geological map of the Sanjiang area showing the major continental blocks and strike-slip faults (modified after Qi et al., 2014).

et al., 1990, 1982). From northwest to southeast, this region is composed of four narrow NW-trending high grade metamorphic belts: the Xuelongshan, Diancangshan and Ailaoshan in Yunnan, and the Day Nui Con Voi (Song Ma) in Vietnam. Due to Cenozoic strike-slip shearing overprints, it is difficult to find the key marker to determine whether this tectonic zone is a suture of Indochina and South China blocks. Recently, high-pressure granulites from Song Ma in Vietnam have been reported, and regarded as a product related to a continental collision setting followed by crustal subduction between the Indochina and South China blocks (Nakano et al., 2008, 2004; Osanai et al., 2004). Ailaoshan metamorphic belt is one of the largest metamorphic belts in the northeastern Indochina Block. The high pressure granulite is one of the key markers to define it as the block convergence boundary. Here, we estimate the pressure/temperature conditions and ages of the high-pressure pelitic granulite in the Ailaoshan metamorphic belt, and then elucidate the relationships between the high-pressure pelitic granulite and events of subduction and collision.

1 GEOLOGICAL SETTING

The Ailaoshan metamorphic belt, 10 to 30 km in width and more than 500 km in length, is located at the southeast of Ailaoshan-Jinshajiang tectonic zone in West Yunnan, China (Fig. 1b), and extends to the northern Vietnam. The Ailaoshan metamorphic belt consists of Xiaoyangjie and Along formations. The Xiaoyangjie Formation is composed of schists and gneisses with minor amphibolite. The Along Formation includes biotite-sillimanite-garnet-bearing amphibolite facies and a few granulite facies metapelites, granitic gneiss, marble and amphibolite. The granitic gneiss commonly contains large feldspar porphyroclasts,

similar to those in augen gneisses, which have undergone various degrees of migmatization. The granitoids intrusion mainly occurred in the Mid-Neoproterozoic and Triassic.

The Indochina Block is separated from the Yangtze Block to the east by the Ailaoshan-Jinshajiang (Ailaoshan-Red River) strike-slip fault (e.g., Leloup et al., 1995; Leloup and Kienast, 1993; Schärer et al., 1990; Tapponnier et al., 1990), and from the Baoshan Block to the west by the Lancangjiang strike-slip fault (Fig. 1). From northeast to southwest, an NW-trending high grade metamorphic belt, a low grade metamorphic fold belt and a Mesozoic fold belt crop out in this region (e.g., Qi et al., 2010). The high grade belt comprises amphibolite facies rocks, while the low grade belt is composed of greenschist facies rocks (Leloup et al., 1995; Leloup and Kienast, 1993). Paleozoic and Mesozoic strata are exposed with minor Cenozoic sedimentary rocks, which have been folded and intruded by magmatic units.

The high-pressure pelitic granulite, the focus of this study, traverses the high-grade metamorphic belt at the southeastern margin of the Ailaoshan metamorphic belt, and crops out as a slice of about 500–700 m in thickness, and is separated from the marble lens to the northwest, and from the paragneiss to the southeast by the thrusts respectively (Fig. 2). This granulite is strongly mylonitized with the foliation parallel to that of the paragneiss.

2 PETROLOGY

The high-pressure pelitic granulite is composed of a kyanite-K-plagioclase-rutile inclusions-rich melanocratic layer with quartz-feldspar-rich layer of about 2–50 mm in width. Mineral foliation and lineation of the granulite defined by direction arrangement of sillimanite, biotite and ribbon quartz (Fig. 3a), show that the rock had undergone ductile deformation later.

The melanocratic layer in high-pressure pelitic granulite contains porphyroclastic garnet (25%), sillimanite (17%), feldspar (18%), flaky biotite (13%) and ribbon quartz (27%) with accessory kyanite, sapphirine, spinel (hercynite), rutile, ilmenite, zircon, monazite and apatite (Fig. 3). Furthermore, muscovite, sericite and hydromica in the layer belong to the late secondary minerals (Figs. 3e, 3g). The melanocratic layer shows high SiO_2 (62.43 wt.%–63.44 wt.%), FeO^T ($FeO+Fe_2O_3$, 7.19 wt.%–8.70 wt.%), CaO (0.81 wt.%–1.14 wt.%), K_2O (3.11 wt.%–3.96 wt.%), TiO_2 (0.86 wt.%–1.01 wt.%) and low MgO (2.76 wt.%–3.07 wt.%) contents (Table 1).

The dominant mineral assemblage of the quartz-feldspar-rich layer is garnet (18%), sillimanite (17%), feldspar (23%), quartz (37%) and biotite (5%). Accessory minerals include rutile, ilmenite, zircon and spinel. Compared with the melanocratic layer, the quartz-feldspar- rich layer is characterized by high SiO_2 (66.21 wt.%–66.89 wt.%), FeO^T (6.98 wt.%–7.44 wt.%), CaO (1.08 wt.%–1.49 wt.%) and Na_2O (1.57 wt.%–1.87 wt.%), and low Al_2O_3 (14.89 wt.%–15.32 wt.%), MgO (2.46 wt.%–2.59 wt.%) and K_2O (2.58 wt.%–2.65 wt.%) (Table 1).

Garnet is one of the main porphyroblasts with sizes varying from 0.5 to 4 mm, and contains numerous monophase and multiphase fine-grained inclusions of sillimanite (0.05–0.3 mm), biotite (0.03–0.2 mm), plagioclase (0.05–0.5 mm), K-feldspar (0.03–0.5 mm), rutile (0.01–0.03 mm), monazite (0.01–0.03 mm), zircon (0.01–0.03 mm), quartz (0.01–0.1 mm), and sapphirine (0.03 mm). The multiphase inclusions are composed of fine-grained aggregates
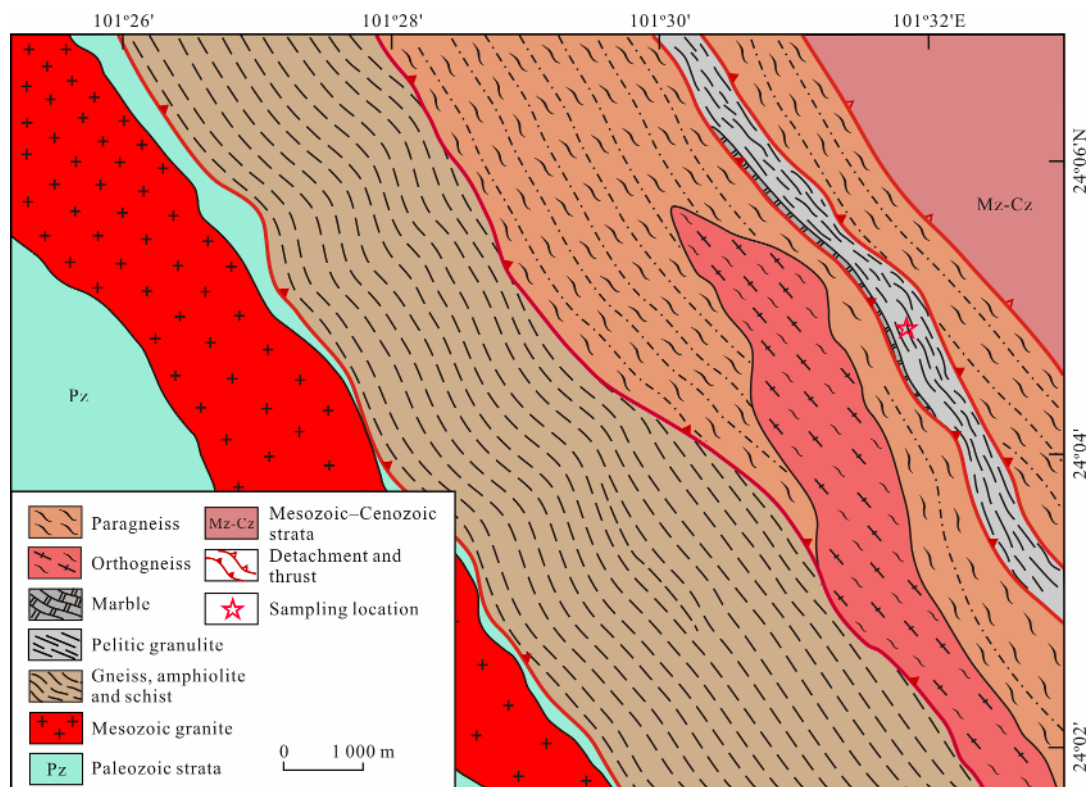
Figure 2. Geological map of the Mid-Neoproterozoic granitoids in the Ailaoshan Orogen (modified after BGMRY, 1990).

Table 1 Major element compositions (wt.%) of the pelitic granulite in the Ailaoshan metamorphic belt

Samples	Melanocratic layer			Leucocratic layer	
	11QHG-2	11QHG-6	11QHG-4	11QHG-5	11QHG-3
SiO_2	63.44	63.22	62.43	66.89	66.21
TiO_2	0.86	0.99	1.01	0.95	0.84
Al_2O_3	16.65	15.66	17.05	14.89	15.32
FeO^T	7.19	8.13	8.7	7.44	6.98
MnO	0.18	0.18	0.21	0.19	0.18
MgO	2.76	3.07	3.07	2.46	2.59
CaO	1.14	0.93	0.81	1.08	1.49
Na_2O	1.57	1.56	1.02	1.57	1.87
K_2O	3.96	3.89	3.11	2.58	2.65
P_2O_5	0.06	0.1	0.17	0.06	0.1
H_2O^+	1.09	1.56	1.98	1.36	1.36
CO_2	0.45	0.19	0.09	0.26	0.09
LOI	0.82	1.26	1.39	0.84	0.76

of sillimanite+plagioclase+biotite, plagioclase+quartz+kyanite+spinel, biotite+quartz and sillimanite+sapphirine. Moreover, a series of sub-parallel fractures within the garnet are obliquely aligned to the major foliation of the granulite, and filled by biotite (or hydromica) or biotite+quartz, biotite+quartz+plagioclase assemblages (Fig. 3h).

Biotite (Bt) shows three modes of occurrences in granulite. Bt-1 exist as flaky subhedral to anhedral inclusions within garnet and feldspar porphyroblasts, or multiphase inclusions coexist with sillimanite, quartz, suggesting it was formed at the same time with garnet and feldspar porphyroblast; Bt-2 occurs as coarse-grained subhedral to anhedral flakes together with garnet, sillimanite and feldspar (Figs. 3a, 3b); alternatively, Bt-2 exist as small anhedral flakes crystal with feldspar, quartz, sillimanite and ilmenite in matrix (Figs. 3a, 3b, 3f, 3g), which may be directly linked to deformation showed later; Bt-3 is distributed as anhedral crystals along the fractures within garnet (Fig. 3h), suggesting it is related to liquid formed in retrograde metamorphism, and in equilibrium with garnet in fractural margin. In each of them, three generations can be marked: the first (Bt-1) formed together with garnet and feldspar porphyroblasts; the second (Bt-2), the biotite formed in the first generation was modified and re-equilibrated with the porphyroblasts in the late metamorphism; and the third (Bt-3), coexisted with quartz and plagioclase sometimes, formed in superimposed metamorphism.

Feldspar (Fsp) shows three modes of occurrence in the granulite: Fsp-1 occur as subhedral to anhedral mineral inclusions (0.01–0.3 mm) in garnet, which is dominated by plagioclase, or coexists with quartz sometimes; Fsp-2 occur as anhedral porphyroblast (0.5–2 mm), surrounded with fine-gained matrix minerals. It is composed of plagioclase, K-feldspar, perthite (per) and anti-perthite (anti-per) (Fig. 3c). The albite occurs as fine-veined lamella in K-feldspar as perthite, and the K-feldspar occurs as schistic lamella in plagioclase as anti-perthite, which can be derived from the exsolution. They occur mainly around fine grained quartz, suggesting the possible presence of a quartz-feldspathic melt. Fsp-3, comprising K-feldspar and plagioclase, occur as fine grained anhedral crystal together with quartz, biotite and minor sillimanite in the matrix and fractures within garnet.

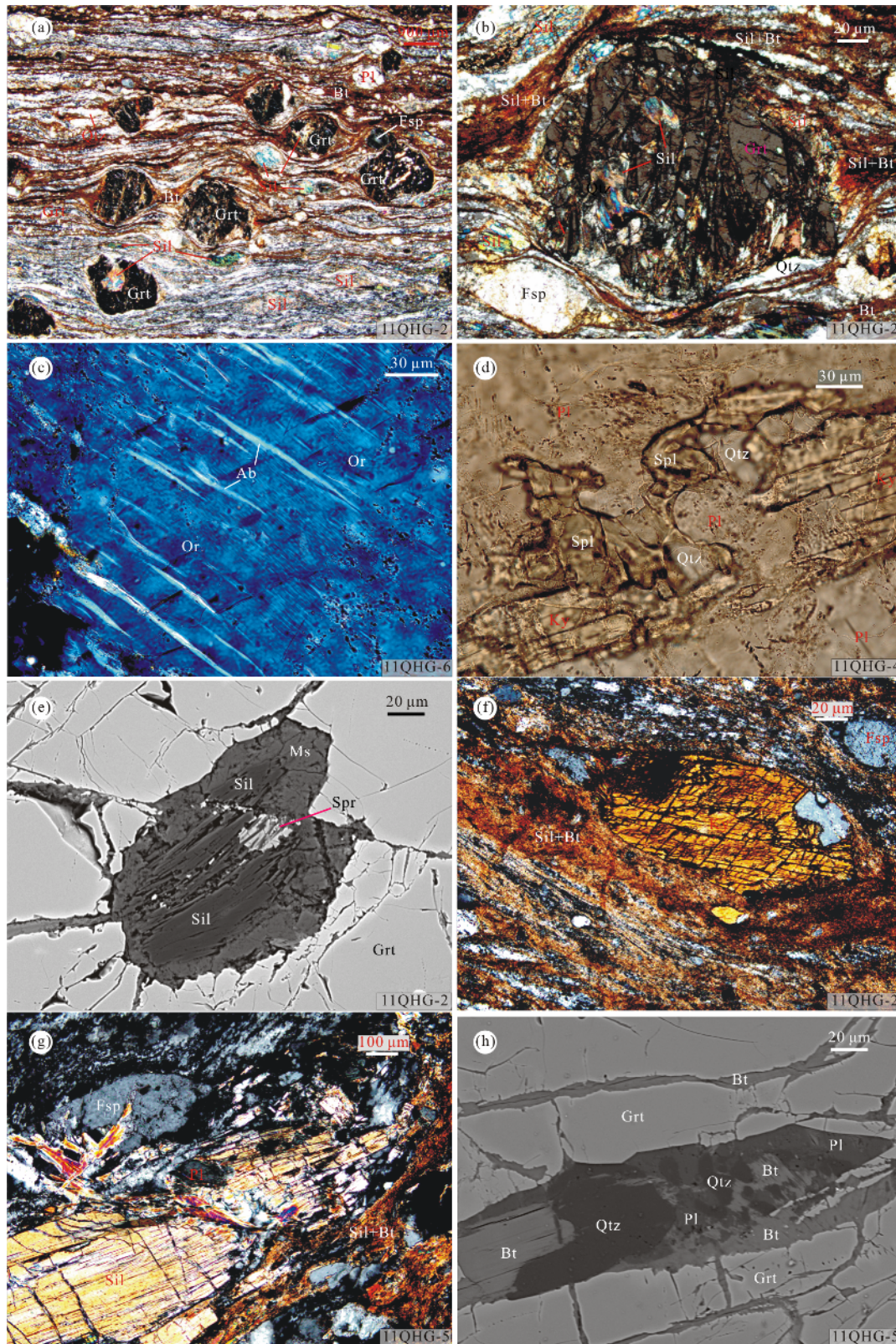Sillimanite appears mainly as needle-shaped aggregate,

Figure 3. Photographraphs showing the characteristic mineral assemblages of the pelitic high-pressure granulites in Ailaoshan metamorphic belt. Photomicrographs showing, (a) the assemblage of garnet (Grt), sillimanite (Sil), feldspar (Fsp), biotite (Bt) and quartz (Qtz) in melanocratic domains of granulite under polarized light; (b) the sillimanite inclusions within the porphyroblast of garnet, which was surrounded by sillimanite, biotite and quartz bands under crossed polarized light; (c) perthite under crossed polarized light; (d) the inclusions of kyanite (Ky) with spinel and quartz in plagioclase (Pl) porphyroblast under polarized light; (e) BSE image of sillimanite and sapphirine (Spr) inclusions rimmed by hydromuscovite within garnet porphyroblast; and photomicrographs showing (f) kyanite porphyroblast surrounded by sillimanite and biotite under crossed polarized light; (g) the muscovite (Ms) filled in the fractures of sillimanite and feldspar under crossed polarized light; (h) BSE image of biotite, plagioclase and quartz assemblage along fractures within garnet. Spl. Spinel; Ab. albite; Or. orthoclase.

partly as a lath-shaped crystal (Figs. 3a, 3b, 3g) with kyanite pseudomorph, and as inclusions within garnet (Figs. 3b, 3e). As shown in Fig. 3g, it is in contact with porphyroclastic garnet, K-feldspar and plagioclase, although most of them are surrounded by fine-grained matrix minerals, indicating they are in equilibrium with them. Kyanite preserves as inclusion within plagioclase (Fig. 3d), or as porphyroblast surrounded by needle-shaped sillimanite and sillimanite+biotite which show the kyanite was replaced by sillimantite (Fig. 3f). The kyanite within feldspar is partially replaced by the spinel (hercynite)+ quartz (Fig. 3d), which suggests the following common decompression reaction: Ky+Grt→Spl+Qtz. The sapphirine occurs as a small spheroid (25 μm) or droplet (5 μm) included in sillimanite and garnet (Fig. 3e). Given the phase relationships in thin sections studied, garnet has most likely supplied Fe and Mg for the formation of the sapphirine.

To sum up, the high-pressure pelitic granulite is composed of porphyroblast and matrix; the matrix was formed by exhausting pre-existing feldspar, quartz, biotite and sillimanite, and which is thought to be directly linked to deformation. This texture shows that garnet, kyanite, feldspar, biotite and rutile inclusions are pre-existing minerals in equilibrium, and belong to the first generation of mineral assemblages (e.g., Dong et al., 2018). Then they experienced modification to get re-equilibrium during decompression at isothermal or increasing temperature condition. The garnet was re-crystallized, and its composition zone disappeared. The kyanite was converted to sillimanite, or to spinel+quartz except a few inclusions in plagioclase, or to sapphirine by reaction with garnet. The biotite was partly dehydrated to sillimanite+liq (melt). The feldspar is rarely involved in the reactions and usually in equilibrium with other minerals. The mineral assemblage of garnet, sillimanite, spinel, sapphirine, K-feldspar, plagioclase, biotite, quartz, rutile, as porphyroblast or in equilibrium with porphyroblast, belongs to the second generation. Together with the first generation, they formed in the first stage. After that, liquid extracted and crystallized during superimposed metamorphism, Grt+liq (melt)→Bt (Bt-3)+Pl (Fsp-3)+Qtz, Sil+liq→Ms. The assemblage of garnet, biotite, muscovite, plagioclase, quartz within fractures of garnet and matrix belongs to the third generation formed in the second metamorphic stage.

3 ANALYTICAL METHODS

Whole-rock major elements were analyzed at the National Research Center for Geoanalysis, Chinese Academy of Geological Sciences, Beijing. Major element oxides were determined using ICP-AES (PE8300). The analytical uncertainty was <0.5%. Analyses of chemical compositions of the constituent minerals were performed on JEOL JXA-8100 wavelength-dispersive electron microprobe at the State Key Laboratory of Continental Tectonics and Dynamics, Beijing. The accelerating voltage was 15 kV, and the beam current was 20 nA.

Zircons were separated from whole-rock samples by a combination of density techniques and handpicking under an electron microscope. The grains were mounted in epoxy, polished to about half of their thickness, and photographed under transmitted and reflected light. Cathodoluminescence (CL) imaging of the zircon grains was carried out in a scanning electron microprobes at the Beijing SHRIMP Center, Chinese Academy of Geological Sciences. The U-Pb dating of the zircons was conducted synchronously by laser ablation inductively coupled plasma-mass spectrometry (LA-ICP-MS) at the State Key Laboratory of Geological Processes and Mineral Resources, Faculty of Earth Sciences, China University of Geosciences (Wuhan) using Agilent 7500a. The GeoLas 2005 laser ablation system was used after the analytical methods and procedures by Hu et al. (2012) and Qi et al. (2012).

4 MINERAL CHEMISTRY

4.1 Garnet

The garnet in Ailaoshan pelitic granulite is a solid solution of almandine (Alm)-pyrope (Pyr)-grossular (Grs)-spessartine (Sps), with almandine component always more than 60 mol% and spessartine component less than 5 mol%. Compositional profiles were measured across representative crystal of garnets. The profiles exhibit compositional plateaus with relatively high Pyr and low Alm values encompassing most of the interior crystals with $Alm_{59-60}Pyr_{34-35}Grs_{4-5}Sps_{1-2}$, and relatively high Alm and low Pyr values in the rim (including the fractural rim) of the crystal with $Alm_{61-71}Pyr_{22-33}Grs_{4-5}Sps_{2-3}$ (Table 2, Fig. 4). It shows the garnet had been homogenized at high temperature metamorphism.

4.2 Biotite

The first two generations of biotite (Bt-1 and Bt-2) are characterized by high TiO_2 content (3.51 wt.%–5.40 wt.%) and low MgO content (9.41 wt.%–14.29 wt.%). The X_{Mg} values $[X_{Mg}=(Mg^{2+}/(Mg^{2+}+Fe^{2+})]$ range from 0.47 to 0.65. On the contrary, biotite of the third generation (Bt-3) has lowest TiO_2 contents (0.56 wt.%–0.75 wt.%) (Table 2).

4.3 Feldspar

K-feldspar in the occurrences of porphyroblast, matrix and lamella in plagioclase shows similar compositional characteristic of high Or content as $Ab_{9-13}An_{0-1}Or_{87-91}$ (An. anorthite) (Table 3). As porphyroblast and matrix, plagioclases have slightly lower anorthite content with $Ab_{65-68}An_{31-34}Or_{0-1}$ compared to that as inclusions with $Ab_{58-62}An_{37-42}Or_{0-1}$. The plagioclase lamella in K-feldspar has higher albite content as $Ab_{91-98}An_{1-2}Or_{1-7}$ (Table 3).

4.4 Other Minerals

Spinel is hercynite-rich (X_{Mg}=0.27–0.28) with negligible amounts of Cr_2O_3 and MnO (Table 4), and its ZnO content reaches up to 4.96% (X_{Zn}=0.12–0.13), together with quartz in contact with the kyanite within plagioclase (Fig. 3e). Sapphirine is characterized by high FeO contents (20.37 wt.%–24.72 wt.%) and low MgO contents (MgO=2.79 wt.%–3.37 wt.%, X_{Mg}=0.19–0.21) (Table 4). The sapphirine shows the high Si contents (0.94–1.84 p.f.u.) consistent with that in association with quartz (Tsunogae and Santosh, 2006; Ouzegane and Boumaza, 1996). Sillimanite is nearly homogeneous content in terms of Al_2O_3 and SiO_2 with minor FeO and Cr_2O_3 for all occurrences (Table 4).

5 METAMORPHIC P-T CONDITIONS

Several geothermobarometers based on the experimental, empirical and thermodynamic parameters using different
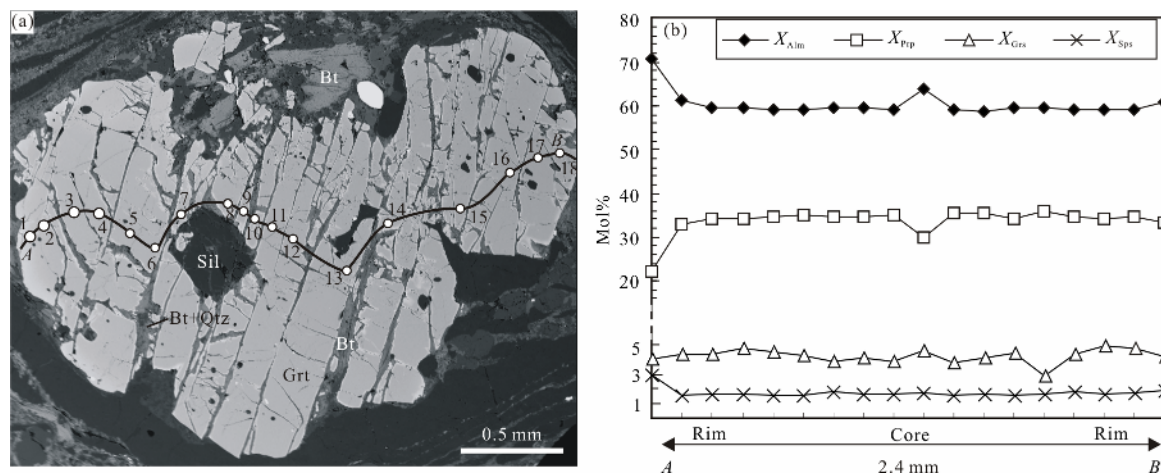
Table 2 Representative electron microprobe analyses data (wt.%) of garnet (O=12) and biotite (O=22)

Spot	Gt-1	Gt-2	Gt-4	Gt-5	Gt-10	Gt-11	Bt2-6	Bt3-18	Bt2/1-9	Bt2/3-4	Bt2-4	Bt2/2-13	Bt2/4-7	Bt6-5
Domain/contact mineral	Rim	Rim	Mantle	Mantle	Core	Core	/Grt+Qtz	/Pl+Grt	/Kf	/Grt+Sil	/Matrix	Inc	Fra	Rim/Qz+Fsp
SiO_2	38.58	39.1	39.06	39.26	38.48	39.21	36.34	35.47	36.71	37.97	37.28	37.45	37.93	36.12
TiO_2	0	0.03	0.03	0	0.04	0	3.78	4.61	4.36	3.51	4.66	4.63	0.56	2.38
Al_2O_3	21.12	21.57	21.55	21.53	21.34	21.6	17.89	16.42	17.36	17.87	17.5	15.74	18.83	16.91
FeO	32.48	29.04	28.39	28.35	29.69	28.37	15.56	19.12	15.39	16.27	14.9	15.36	16.8	17.47
Cr_2O_3	0.01	0	0.03	0.03	0.05	0.05	0.09	0.04	0.05	0.03	0.03	0.02	0.04	0.05
MnO	1.29	0.72	0.76	0.72	0.78	0.73	0.06	0.04	0.05	0.05	0	0.02	0.04	0.07
MgO	5.55	8.5	8.88	9.09	7.57	9.2	12.03	9.82	11.27	10.12	11.73	12.92	11.05	13.25
CaO	1.39	1.58	1.73	1.64	1.63	1.38	0	0	0.02	0.02	0.04	0.02	0.01	0.09
Na_2O	0	0.01	0.02	0.01	0.02	0.01	0.14	0.06	0.12	0.09	0.13	0.18	0.11	0.09
K_2O	0	0.01	0	0	0.02	0.03	9.54	9.57	9.59	9.21	9.7	9.11	9.16	8.59
Total	100.42	100.61	100.44	100.63	99.62	100.57	95.43	95.13	94.93	95.13	95.97	95.46	94.55	95.03
			O=12 for garnet							O=22 for biotite				
Si	3.04	3.01	3.01	3.02	3.01	3.01	5.43	5.43	5.51	5.66	5.51	5.57	5.69	5.45
Ti	0	0	0	0	0	0	0.42	0.53	0.49	0.39	0.52	0.52	0.06	0.27
Al	1.96	1.96	1.96	1.95	1.97	1.95	3.15	2.96	3.07	3.14	3.05	2.76	3.33	3
Fe^{2+}	2.14	1.87	1.83	1.82	1.94	1.82	1.94	2.45	1.93	2.03	1.84	1.91	2.11	2.2
Mn	0.09	0.05	0.05	0.05	0.05	0.05	0.01	0.01	0.01	0.01	0	0	0	0.01
Mg	0.65	0.98	1.02	1.04	0.88	1.05	2.68	2.24	2.52	2.25	2.58	2.87	2.47	2.98
Ca	0.12	0.13	0.14	0.13	0.14	0.11	0	0	0	0	0.01	0	0	0.01
Na	0	0	0	0	0	0	0.04	0.02	0.03	0.03	0.04	0.05	0.03	0.03
K	0	0	0	0	0	0	1.82	1.87	1.83	1.75	1.83	1.73	1.75	1.65
X_{Mg}	0.23	0.34	0.36	0.36	0.31	0.37	0.58	0.48	0.57	0.53	0.58	0.6	0.54	0.61
X_{Alm}	70.82	61.13	59.39	59.11	63.76	59.27								
X_{Prp}	22.24	32.89	34.15	34.82	29.88	35.31								
X_{Grs}	4	4.4	4.79	4.51	4.61	3.82								
X_{Sps}	2.93	1.58	1.67	1.56	1.75	1.6								

X_{Alm}, X_{Prp}, X_{Grs}, X_{Sps} are the mole percent of almandite, pyrope, grossular and spessartine; inc. inclusion; fra. distributed within fracture.

Table 3 Representative electron microprobe analyses data (wt.%) of feldspar (O=8) (b. porphyroblast; inc. inclusion)

Spot	1-2	3-1	3-8	2-2	11/6-11	11/6-4	3-13	2/1-5	2/1-1	4-7	11/2-1	11/2-5
Min.	Kf/b	Kf/matrix	Kf/Sil	Kf/Grt-trail	Anti-per/Pl	Anti-per/Kf	Pl/matrix	Pl/inc	Pl/Sil-trail	Pl/inc	Per/Ab	Per/Or
SiO_2	65.64	66.29	65.67	66.61	61.52	64.70	61.55	61.06	62.14	59.54	67.52	64.20
TiO_2	0.03	0.04	0.05	0.01	0.04	0.02	0.00	0.02	0.00	0.02	0.00	0.02
Al_2O_3	18.61	17.96	18.01	17.52	24.08	18.35	24.11	24.39	24.10	25.22	19.76	18.32
FeO	0.02	0.10	0.02	0.28	0.01	0.00	0.00	0.01	0.00	0.36	0.00	0.02
Cr_2O_3	0.03	0.00	0.00	0.00	0.01	0.00	0.00	0.01	0.01	0.00	0.00	0.02
MnO	0.01	0.02	0.00	0.00	0.04	0.01	0.04	0.00	0.01	0.01	0.02	0.00
MgO	0.00	0.00	0.00	0.01	0.00	0.00	0.02	0.01	0.07	0.01	0.01	0.00
CaO	0.08	0.05	0.04	0.02	5.69	0.09	6.33	6.83	6.88	7.68	0.37	0.12
Na_2O	1.22	0.99	1.04	1.47	8.01	1.43	7.70	7.19	7.22	6.98	11.26	1.34
K_2O	14.73	14.71	14.89	14.68	0.24	14.43	0.25	0.25	0.23	0.19	0.20	15.00
Total	100.37	100.16	99.76	100.59	99.64	99.02	99.99	99.78	100.67	100.04	99.15	99.04
O=8												
Si	3.00	3.03	3.02	3.04	2.74	3.00	2.73	2.72	2.74	2.66	2.98	2.99
Ti	0.00	0.00	0.00	0.00	0.00	0.00	0.00	0.00	0.00	0.00	0.00	0.00
Al	1.00	0.97	0.98	0.94	1.26	1.00	1.26	1.28	1.25	1.33	1.03	1.00
Fe^{2+}	0.00	0.00	0.00	0.01	0.00	0.00	0.00	0.00	0.00	0.01	0.00	0.00
Mn	0.00	0.00	0.00	0.00	0.00	0.00	0.00	0.00	0.00	0.00	0.00	0.00
Mg	0.00	0.00	0.00	0.00	0.00	0.00	0.00	0.00	0.00	0.00	0.00	0.00
Ca	0.00	0.00	0.00	0.00	0.27	0.00	0.30	0.33	0.33	0.37	0.02	0.01
Na	0.11	0.09	0.09	0.13	0.69	0.13	0.66	0.62	0.62	0.60	0.96	0.12
K	0.86	0.86	0.87	0.85	0.01	0.85	0.01	0.01	0.01	0.01	0.01	0.89
Ab	11	9	10	13	71	13	68	65	65	62	97	12
An	0	0	0	0	28	0	31	34	34	37	2	1
Or	89	91	90	87	1	87	1	1	1	1	1	87

Figure 4. Compositional profiles of garnet porphyroblast. Alm. Almandine; Prp. pyrope; Grs. grossularire; Sps. spessartine.

composition-activity models for the various minerals are applicable for high-grade metamorphic rocks due to the presence of a number of ferromagnesian minerals, such as garnet-biotite geothermometer (Holdaway, 2000), garnet-Al silicate-plagioclase (GASP) geobarometer (Koziol and Newton, 1988), and garnet-biotite-plagioclase-quartz (GBPQ) geothermobarometer (Wu et al., 2018, 2004).

Here, the *P-T* conditions were estimated by GBPQ geo-

thermobarometer (Wu et al., 2004) using the compositions of host minerals re-equilibrated at the initial stage of retrograde metamorphism or occurred along fractures within garnet at late stage of retrograde metamorphism. The results show that the *P-T* ranges of the second and third generations are 8.6–10.4 kbar at 850–919 ℃ and 3.5–3.9 kbar at 572–576 ℃, respectively. The top temperature (920 ℃) for the second generation is slightly higher than the upper limit of the GBPQ geothermobarometery,

Table 4　Representative electron microprobe analyses data (wt.%) of sillimanite (O=5), spinel (O=4) and sapphirine (O=20)

Spot	3-10	4-14	1-19	3-22	2-9	11/5-1	11/5-2	3-53	3-54	3-55
Mineral	Sil (b)	Sil (pil)	Sil (m)	Sil (fib)	Sil (inc)	Spl (inc/Pl)		Spr (inc/Sil)	Spr (inc/Sil)	Spr (inc/Sil)
SiO_2	37.42	38.08	38.20	37.92	37.84	0.04	0.02	15.41	14.75	14.09
TiO_2	0.01	0.00	0.02	0.01	0.00	0.00	0.01	0.00	0.00	0.00
Al_2O_3	61.84	60.69	60.44	60.86	61.64	61.22	61.16	59.41	59.05	56.09
FeO	0.18	0.27	0.34	0.30	0.30	27.10	27.21	20.37	21.84	24.72
Cr_2O_3	0.02	0.08	0.02	0.06	0.01	0.12	0.08	0.10	0.08	0.11
MnO	0.01	0.00	0.00	0.00	0.00	0.13	0.10	0.05	0.07	0.10
MgO	0.01	0.02	0.01	0.00	0.02	5.61	6.03	3.03	2.79	3.37
CaO	0.00	0.01	0.02	0.01	0.01	0.02	0.00	0.03	0.03	0.09
Na_2O	0.00	0.01	0.01	0.01	0.02	0.17	0.17	0.04	0.00	0.05
K_2O	0.01	0.00	0.00	0.01	0.01	0.00	0.00	0.03	0.09	0.17
NiO	0.00	0.00	0.00	0.00	0.00	0.10	0.10	0.00	0.00	0.00
ZnO	0.00	0.00	0.00	0.00	0.00	4.64	4.96	0.00	0.00	0.00
Total	99.74	99.14	99.07	99.21	99.87	99.14	99.83	98.46	98.69	98.78
O=20										
Si	1.02	1.04	1.04	1.03	1.02	0.00	0.00	0.98	0.94	1.84
Ti	0.00	0.00	0.00	0.00	0.00	0.00	0.00	0.00	0.00	0.00
Al	1.97	1.95	1.94	1.95	1.96	2.00	1.99	4.44	4.44	8.61
Fe^{2+}	0.00	0.01	0.01	0.01	0.01	0.63	0.63	1.08	1.17	2.69
Mn	0.00	0.00	0.00	0.00	0.00	0.00	0.00	0.00	0.00	0.01
Mg	0.00	0.00	0.00	0.00	0.00	0.23	0.25	0.29	0.27	0.65
Ca	0.00	0.00	0.00	0.00	0.00	0.00	0.00	0.00	0.00	0.01
Na	0.00	0.00	0.00	0.00	0.00	0.01	0.01	0.00	0.00	0.01
K	0.00	0.00	0.00	0.00	0.00	0.00	0.00	0.00	0.01	0.03
Ni	0.00	0.00	0.00	0.00	0.00	0.00	0.00	0.00	0.00	0.00
Zn	0.00	0.00	0.00	0.00	0.00	0.12	0.13	0.00	0.00	0.00
X_{Mg}	0.07	0.11	0.05	0.00	0.00	0.27	0.28	0.21	0.19	0.20
X_{Fe}	0.93	0.89	0.95	1.00	1.00	0.64	0.63	0.79	0.81	0.80
X_{Zn}	0.00	0.00	0.00	0.00	0.00	0.12	0.13	0.00	0.00	0.00

X_{Mg}=Mg/(Fe^{2+}+Mg); X_{Zn}=Zn/(Fe^{2+}+Mg+Zn); pil. pillar crystalline; fib. fibrocrystalline; m. matrix; Spl. spinel.

but it is still within its range, and supported by a high temperature mineral assemblage of garnet-sillimanite-feldspar-biotite with high-TiO_2 and FeO contents. According to the maximum temperature and the lower limit of kyanite stability, the pressure is determined to be greater than 12 kbar (Moulas et al., 2013). We therefore suggest the 8.6–12 kbar at 850–920 ℃ and 3.5–3.9 kbar at 572–576 ℃ could represent the P-T condition of the second and third generations of metamorphism respectively.

6　GEOCHRONOLOGY

　　Zircons analyzed in this study were separated from samples (11QHG-3) collected from the melanocratic and leucocratic domains in high-pressure pelitic granulite, respectively. Zircons are euhedral to subhedral, translucent, and prismatic. Most of the zircon grains are 80 to 120 μm long and have aspect ratios ranging from 1.5 to 2.0. Most grains have a core-mantle-rim, core-rim or core-mantle structure (Fig. 5). The mantles and rims with dark-gray homogenous patterns show that the zircons might be formed in multiple metamorphic stages (Figs. 5b, 5c, 5e, 5f). The cores are subhedral to rounded, varying from 20 to 100 μm long with oscillatory zoning (Figs. 5a, 5c, 5e), indicating that they are inherited from older detrital zircons. As shown in Table 5 and Fig. 6, 62 spots of 50 zircons from sample 11QHG-3 were conducted. Among these, 32 spots on zircon cores, yield ^{238}U/^{206}Pb ages of 337 to 2 791 Ma with U and Th contents ranging from 33 ppm to 3 881 ppm and 28 ppm to 1 167 ppm, respectively, and higher Th/U ratios varying from 0.13 to 1.33. Part of them, discordant and distributing inside the concordant line (Fig. 6a), yield ^{206}Pb/^{238}U ages of 1 877 to 440 Ma. These indicate metamictization and lead loss, which could not represent the crystallization age of the inherited detrital zircons. Other concordant analyses, yielding ^{206}Pb/^{238}U ages from 1 871 to 337 Ma (Fig. 6a), could represent the crystallization ages of the inherited zircons. We interpret those ages as the crystallization ages of the inherited detrital zircons (Fig. 6), the youngest ^{238}U/^{206}Pb age of 337 Ma as oldest age for the protolith of the pelitic granulite. Eighteen spots

Table 5 Zircon LA-ICP-MS U-Pb data for the pelitic granulite in the Ailaoshan metamorphic belt

Spot No.	Pb	Th	U	Th/U	$^{207}Pb/^{206}Pb$	1σ	$^{207}Pb/^{235}U$	1σ	$^{206}Pb/^{238}U$	1σ	Age (Ma) $^{206}Pb/^{238}U$	1σ	Location
		(ppm)											
1	19	8	361	0.02	0.049 08	0.001 86	0.034 76	0.001 36	0.005 13	0.000 05	33	0.3	r
2	6	6	407	0.01	0.047 13	0.001 39	0.034 61	0.000 99	0.005 34	0.000 05	34	0.3	r
3	32	4	182	0.02	0.051 86	0.000 62	0.207 41	0.002 93	0.029 01	0.000 24	184	1.5	m
4	6	11	446	0.02	0.047 28	0.001 46	0.031 82	0.000 92	0.004 90	0.000 06	31	0.4	r
5	41	5	349	0.01	0.049 10	0.000 93	0.035 36	0.000 66	0.005 23	0.000 03	34	0.2	r
6	6	8	290	0.03	0.050 50	0.000 35	0.180 49	0.001 57	0.025 90	0.000 11	165	0.7	m
7	3	1	171	0.01	0.051 31	0.000 75	0.147 87	0.002 14	0.020 92	0.000 11	133	0.7	m
8	4	6	370	0.02	0.048 98	0.001 49	0.034 95	0.000 98	0.005 19	0.000 05	33	0.3	r
9	6	11	201	0.05	0.049 19	0.001 99	0.034 90	0.001 31	0.005 17	0.000 04	33	0.3	r
10	261	4	177	0.02	0.048 91	0.000 56	0.120 08	0.001 56	0.017 79	0.000 11	114	0.7	m
11	2	2	167	0.01	0.050 82	0.000 62	0.194 48	0.002 68	0.027 73	0.000 16	176	1.0	m
12	36	3	181	0.02	0.049 43	0.001 24	0.040 31	0.001 08	0.005 95	0.000 06	38	0.4	m
13	3	2	223	0.01	0.051 31	0.000 89	0.159 38	0.002 81	0.022 54	0.000 16	144	1.0	m
14	2	3	185	0.02	0.049 25	0.001 03	0.166 19	0.003 43	0.024 48	0.000 19	156	1.2	m
15	3	9	250	0.04	0.054 76	0.001 54	0.064 96	0.001 52	0.008 64	0.000 13	55	0.8	m
16	99	8	202	0.04	0.047 41	0.002 65	0.032 47	0.001 78	0.005 00	0.000 07	32	0.4	r
17	107	7	457	0.02	0.053 07	0.000 39	0.254 96	0.003 26	0.034 73	0.000 25	220	1.6	m
18	2	7	271	0.02	0.053 31	0.001 92	0.036 53	0.001 42	0.004 96	0.000 05	32	0.4	r
19	50	9	286	0.03	0.048 67	0.001 47	0.034 10	0.001 10	0.005 08	0.000 05	33	0.3	r
20	25	4	170	0.02	0.053 29	0.000 54	0.274 14	0.003 97	0.037 25	0.000 32	236	2.0	m
21	2	8	153	0.05	0.047 66	0.002 27	0.031 80	0.001 50	0.004 85	0.000 04	31	0.28	r
22	461	108	105	1.03	0.229 17	0.000 69	17.124 70	0.187 10	0.541 91	0.005 79	2 791	24.2	c
23	71	70	148	0.47	0.070 71	0.000 50	1.048 36	0.009 42	0.107 52	0.000 64	658	3.7	c
24	72	75	57	1.33	0.067 05	0.000 55	0.834 01	0.010 25	0.090 36	0.000 94	558	5.6	c
25	43	38	33	1.14	0.071 46	0.001 18	1.156 08	0.030 42	0.117 11	0.001 90	714	11.0	c
26	523	129	264	0.49	0.179 79	0.000 49	8.381 43	0.063 16	0.338 04	0.002 25	1 877	10.9	c
27	445	297	233	1.27	0.072 06	0.000 23	1.386 55	0.009 40	0.139 54	0.000 83	842	4.7	c
28	89	28	39	0.72	0.100 03	0.001 15	3.318 14	0.062 05	0.240 67	0.003 92	1 390	20.3	c
29	230	134	199	0.67	0.068 66	0.000 76	1.321 25	0.016 20	0.139 62	0.000 99	842	5.6	c
30	190	71	69	1.03	0.103 60	0.003 64	3.353 55	0.046 24	0.247 92	0.003 07	1 428	15.9	c
31	195	119	138	0.87	0.068 14	0.000 49	1.280 61	0.013 06	0.136 36	0.001 25	824	7.1	c

Table 5 Continued

Spot No.	Pb	Th	U	Th/U	207Pb/206Pb	1σ	207Pb/235U	1σ	206Pb/238U	1σ	Age (Ma) 206Pb/238U	1σ	Location
		(ppm)											
32	101	49	82	0.59	0.086 33	0.000 74	2.593 60	0.041 10	0.217 77	0.002 45	1 270	13.0	c
33	49	29	101	0.29	0.084 98	0.001 32	0.930 32	0.020 60	0.079 44	0.001 38	493	8.2	c
34	36	29	61	0.49	0.066 89	0.001 45	0.676 63	0.019 93	0.073 51	0.001 78	457	10.7	c
35	113	59	129	0.46	0.088 12	0.000 67	1.693 65	0.043 62	0.139 38	0.003 43	841	19.4	c
36	111	85	66	1.29	0.068 16	0.000 96	1.240 12	0.030 62	0.132 01	0.002 87	799	16.4	c
37	12	35	167	0.21	0.047 39	0.002 14	0.028 79	0.001 34	0.004 41	0.000 07	28	0.5	r
38	46	45	77	0.59	0.075 96	0.001 24	1.139 32	0.021 68	0.108 86	0.001 42	666	8.3	c
39	74.7	125	1 116	0.11	0.058 73	0.003 19	0.243 38	0.013 34	0.030 01	0.000 54	191	3.4	m
40	19	23	2 585	0.01	0.047 34	0.003 42	0.059 39	0.004 40	0.009 42	0.000 24	60	1.5	m
41	112	121	1 344	0.09	0.058 45	0.002 80	0.467 91	0.025 58	0.057 34	0.002 21	359	13.5	c
42	36	37	2 296	0.02	0.052 12	0.003 39	0.129 10	0.010 36	0.018 07	0.000 97	115	6.1	m
43	1 861	634	4 737	0.13	0.144 75	0.003 96	5.290 23	0.151 88	0.262 83	0.003 45	1 504	17.6	c
44	76	46	1 208	0.04	0.064 29	0.002 53	0.625 58	0.026 92	0.070 59	0.001 77	440	10.6	c
45	1 595	657	4 413	0.15	0.154 86	0.003 76	4.956 83	0.131 08	0.231 19	0.003 10	1 341	16.2	c
46	611	408	591	0.69	0.121 50	0.003 36	5.616 16	0.193 30	0.334 76	0.007 29	1 861	35.2	c
47	781	759	1 146	0.66	0.094 31	0.003 12	2.477 40	0.091 27	0.190 19	0.003 02	1 122	16.3	c
48	107	135	1 724	0.08	0.061 35	0.003 14	0.423 06	0.025 11	0.049 60	0.001 19	312	7.3	c
49	21	53	4 243	0.01	0.053 83	0.003 72	0.042 69	0.003 03	0.005 78	0.000 13	37	0.8	r
50	633	527	1 667	0.32	0.125 53	0.003 48	3.403 83	0.126 70	0.194 83	0.005 01	1 147	27.1	c
51	74	93	1 833	0.05	0.068 41	0.003 04	0.257 18	0.014 29	0.026 81	0.000 99	171	6.2	m
52	17	29	2 225	0.01	0.049 89	0.004 14	0.071 91	0.006 88	0.010 21	0.000 43	66	2.7	m
53	94	167	948	0.18	0.056 94	0.003 13	0.442 50	0.028 30	0.053 66	0.001 94	337	11.8	c
54	28	33	1 690	0.02	0.053 74	0.003 10	0.144 15	0.009 10	0.019 18	0.000 58	122	3.7	m
55	131	109	1 712	0.06	0.064 98	0.003 02	0.492 15	0.025 49	0.053 60	0.001 28	337	7.8	c
56	250	52	2 439	0.02	0.067 46	0.002 15	1.149 98	0.035 96	0.121 46	0.001 30	739	7.5	c
57	701	527	2 110	0.25	0.082 89	0.002 77	2.284 76	0.091 76	0.195 23	0.004 53	1 147	27.1	c
58	32	18	1 410	0.01	0.050 67	0.003 01	0.208 99	0.011 81	0.029 87	0.000 55	190	3.4	m
59	898	357	3 881	0.09	0.096 08	0.002 79	2.652 92	0.086 60	0.195 97	0.003 93	1 154	21.2	c
60	316	262	471	0.56	0.104 07	0.003 46	3.791 44	0.127 08	0.258 69	0.003 62	1 483	18.5	c
61	1 084	488	2 102	0.23	0.137 36	0.004 72	5.176 39	0.295 40	0.251 52	0.009 29	1 446	47.8	c
62	537	1 167	934	1.25	0.068 60	0.002 87	0.721 46	0.031 06	0.075 63	0.001 81	470	10.9	c

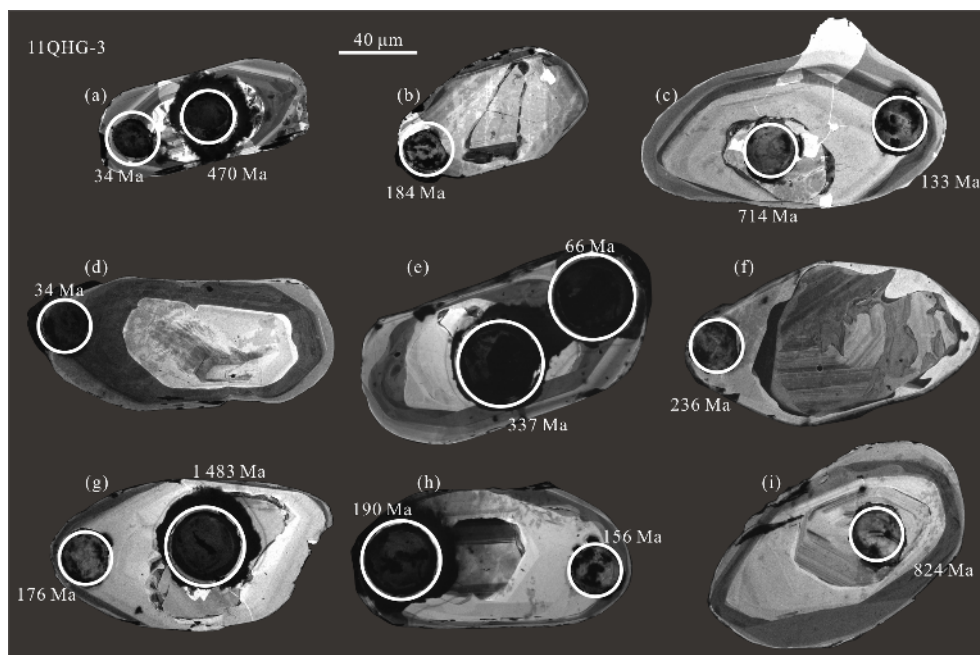Notes: c. core; m. mantle; r. rim.

Figure 5. CL images and U-Pb ages for zircons from the granulite from the Ailaoshan metamorphic belt.
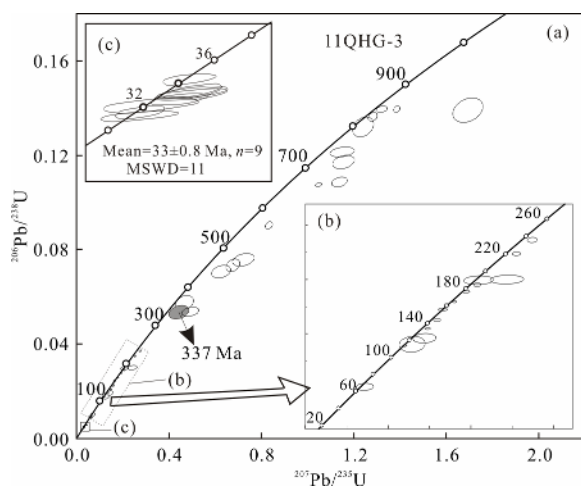

Figure 6. Zircon U-Pb concordia diagram of the granulite from the Ailaoshan metamorphic belt.

on zircon mantles yield $^{238}U/^{206}Pb$ ages of 66 to 236 Ma with U and Th contents of 167 ppm–2 585 ppm and 1 ppm–125 ppm, respectively, and lower Th/U ratios of 0.01 to 0.05 except spot 39, and distributed on the concorde line (Fig. 6b). Thirteen spots on zircon rims yield $^{238}U/^{206}Pb$ ages range from 28 to 38 Ma. Among these, 3 spots (spots 12, 37 and 49 yield slightly younger or elderly $^{206}Pb/^{238}U$ ages of 28±0.5, 37±0.8 and 38±0.4 Ma). Ten spots are concordant, and yield a weighted mean age of 33±0.8 Ma (MSWD=11) (Fig. 6c) with similar U and Th contents and Th/U ratios to zircon mantles.

7 DISCUSSION
7.1 Metamorphic Evolution

The detailed petrographic and compositional features of minerals indicate various reactions at both prograde and retrograde metamorphism in Ailaoshan pelitic granulite, such as: (1) sillimanite with kyanite pseudomorph, and minor kyanite as in-

clusion within plagioclase, illustrated that the metamorphic condition changed from the kyanite to the sillimanite stability fields, and the reaction occurred during prograde metamorphism: Ky→Sil. (2) Kyanites as inclusions within plagioclase were partially replaced by spinel (hercynite)+quartz, suggesting the following common decompression reaction: Ky+Grt→Spl (Her)+ Qtz. (3) Small spherical and drop shaped sapphirine distributed in sillimanite and garnet, shows the reaction: Grt+Sill (Ky)→Spr. (4) As shown in Figs. 3h and 4, the homogeneous compositional section, except the iron enrichment at the rims adjacent to biotite and fractures filled by biotite±quartz±plagioclase, shows the garnet has been homogenized at peak metamorphism, and undergone the Fe-Mg exchange reaction between garnet and biotite or liquid (melt) during retrograde metamorphism, and had re-equilibrated each other with the reaction: Grt+liq (melt)→ Bt±Qtz±Pl. (5) Per/anti-Per during decreasing temperature. These indicate the pelitic granulite has experienced two stages of peak to initial retrograde, and late superimposed metamorphism. Based on the equilibrium mineral assemblage and GBPQ geothermobarometery, we estimate P-T at 8.6–12 kbar, 850–920 °C as the initial retrograde metamorphic conditions, which are corroborated by critical UHT assemblages of Grt+Sil+Spl+Spr+ Bt+Rut. At the same time, we take the P-T of 3.5–3.9 kbar, 572–576 °C for the condition of final metamorphic stage based on the mineral assemblage of Pl+Bt+Qtz filling in the fractures of garnet.

Temperatures estimated for sapphirine-spinel assemblages have been reported from garnet-sillimanite-spinel quartzofeldspathic gneisses at Skallen and Langhovde in Lützow-Holm Bay (Motoyoshi et al., 1985; Hiroi et al., 1983), Rundsvågshetta (Motoyoshi and Ishikawa, 1997; Motoyoshi et al., 1989), and the Highland Complex in Sri Lanka (Hiroi et al., 1994; Ogo et al., 1992). The experimental results (Bertrand et al., 1991; Hensen and Green, 1972) demonstrated temperatures of 900–1 050 °C and pressures of 11–12 kbar for the sapphirine bearing assem-

blage. However, the phase relations of very small spinel and sapphirine distributed around kyanite and sillimanite, the low pressure spinel with high Zn content (Harley, 2008), and the sapphirine with high FeO content and low X_{Mg} values (<0.21), are different from UHT granulite above. These show the mineral assemblage of the spinel and sapphirine formed by the metastable reaction of garnet and kyanite under the *P-T* conditions of 5–7 kbar and 580–800 ºC (Moulas et al., 2013) during the uplift stage of the pelitic granulite. Hence, we can't estimate the peak meta-morphic *P-T* condition with sapphirine and spinel. Detailed in-vestigations on mineral inclusions within porphyroblastic garnet and feldspar are required to evaluate the peak metamorphic con-dition and understand the *P-T* path. Zircon LA-ICP-MS U-Pb dating shows that there are three age groups from zircon core, mantle and rim, respectively. Among them, we suggest the con-cordant ages of the zircon cores as the crystallization ages of the inherited zircons, and the youngest $^{238}U/^{206}Pb$ age of 337 Ma (spot 54) as the oldest age for the protolith of the pelitic granulite. The second age group from the zircon mantles ranges from 236 to 66 Ma. We interpret the oldest age of 236 Ma as the age of the first metamorphic stage, and the reasons are as follows: (1) The CL images show that the zircon mantles have euhedral shapes and homogeneous patterns with rims of 0–40 μm in width (Fig. 5), except spot 54, other metamict ones have the same gray rims (Figs. 5a, 5d), and radiogenic Pb loss during retrograde meta-morphism, including radiation damage, self-annealing and chemical reaction (Nam et al., 2001; Sano et al., 1999; Pidgeon, 1992). (2) Partial spots containing mantles and rims, yield mixed $^{238}U/^{206}Pb$ ages (Figs. 5b, 5c, 5e, 5g, 5h). (3) The migmatization represented by an intercalation of felsic leucosomes and restitic melanocratic layers, shows that there are products of liquid or melt, which was related to the dehydration of biotite (Aït-Djafer et al., 2009). Such fluid or melt remaining in communication with the mineral assemblages following UHT has a significant effect on the ages recorded by geochronological systems, even to the extent of producing widespread post-UHT metamorphic zir-con (Harley, 2004). (4) The oldest age of 236 Ma is generally consistent with that of 230–270 Ma reported for high pressure granulites and eclogites of the northeastern Indochina in Vietnam (Nakano et al., 2008, 2007, 2004; Osanai et al., 2004; Nam et al., 2001; Lepvrier et al., 1997). We therefore interpret the oldest age of 236 Ma in the zircon mantle as the age for the first stage of metamorphism. The third age group from the zircon rims of 38 to 28 Ma is consistent with the ages of the ductile shearing along the Ailaoshan metamorphic belt (35–21 Ma) estimated by zircon U-Pb and amphibole, muscovite, biotite and K-feldspar Ar-Ar dating (Liu et al., 2015; Tang et al., 2013; Cao et al., 2011a, b; Liang et al., 2007; Searle, 2006; Leloup et al., 1995). Combining *P-T* conditions of the second retrograde metamorphic stage simi-lar to the ductile shearing *P-T* conditions of 480 ºC at 3 kbar to 650 ºC at 5 kbar (Wu et al., 2017; Liu et al., 2012; Nam et al., 1998; Leloup and Kienast, 1993), we suggest the weighted mean age of 33 Ma of the zircon rims as the age of the second meta-morphic stage.

It is inferred that the high-pressure pelitic granulite in Ailaoshan Orogen has experienced multiple tectonothermal events. The upper continental crust subducted to the middle-lower crust, and underwent granulite facies metamorphism, then exhumed to the middle-upper crust quickly and initial retrograde metamorphism occurred at 8.6–12 kbar at 850–920 ºC (about 236 Ma), and final second stage of metamorphism overprinted at the condition of 3.5–3.9 kbar at 572–576 ºC since 33 Ma (Fig. 6).

7.2 Tectonic Implications

The LA-ICP-MS U-Pb ages for zircon cores consist of a Early Paleozoic group and a Precambrian group (Table 5). The Precambrian ages can be further divided into Neoproterozoic and Mesoproterozoic populations. In general, the orderless distribution of these ages shows their detrital zircons origin in the rocks from Mesoproterozoic to Lower Carboniferous, and implying that the protolith of the granulite is a pelitic sedimentary rock formed after Early Carboniferous. The *P-T* condition of peak metamorphism shows that the granulite formed in the lower continental crust (≥30 km). It means that the pelite had been brought down to the lower continental crust. How and when was it brought to the lower crust? There are two tectonothermal events in Ailaoshan Orogen since Paleozoic: (1) The amalgamation of the South China and Indo-china blocks during the Early to Middle Triassic (Jian et al., 2009; Yumul et al., 2008; Owada et al., 2007; Trung et al., 2006; Lep-vrier et al., 2004; Sengör, 1984). It was supported by numerous Carboniferous ophiolitic mafic-ultramafic blocks regarded as relics of the Paleo-Tethys oceanic crust (Jian et al., 2008, 1998; Metcalfe, 2002; Zhang et al., 1995, 1994), an island arc volcano-sedimentary zone (Dong et al., 2000; Mo et al., 1993) and the Upper Triassic molasse at the southwestern margin of the Ailaoshan Orogen, China, and HP-UHP granulites and eclogite from northern Vietnam (Nakano et al., 2010, 2008; Lepvrier et al., 2004; Osanai et al., 2004). (2) The large scale sinistral slip-shearing resulted from the convergence between India and Asia, and the southeastward extrusion of Indochina Block related to the South China Block since the Early Cenozoic (Searle et al., 2010; Yeh et al., 2008; Morley, 2002; Leloup et al., 1995; Tapponnier et al., 1990, 1982). The age of the peak metamorphism recorded by the oldest age of zircon mantle at 236 Ma and that of the super-imposed metamorphism recorded by a weighted mean age of zircon rim at 33 Ma are consistent with the two tectonothermal events respectively. So we speculate that the sedimentary rock in Ailaoshan metamorphic belt was subducted/underthrusted to the lower continental crust (deeper than 30 km) and experienced granulite-facies metamorphism and partial melting, resulting from the collision of the Indochina and South China blocks during In-dosinian, and superimposed metamorphism since the Oligocene, which is demonstrated by sub-parallel fractures within porphyro-blastic garnet formed by slip shearing.

8 CONCLUSIONS

The high-pressure pelitic granulite has undergone two stages of metamorphism: (1) the peak to initial retrograde metamorphism recorded by the mineral assemblage of garnet, kyanite, K-feldspar, quartz and rutile inclusions and the mineral assemblage of garnet, sillimanite, spinel, sapphirine, K-feldspar, plagioclase, biotite, quartz and rutile, respectively; (2) the su-perimposed metamorphism recorded by the mineral assemblage of biotite, plagioclase, quartz and ilmenite.

The initial retrograde metamorphism occurred at 8.6–12 kbar at 850–920 ºC in Indosinian (about 235 Ma), and is related

to the amalgamation of the South China and Indochina blocks during the Triassic. The late superimposed metamorphism occurred at the *P-T* condition of 3.5–3.9 kbar at 572–576 ℃ since Oligocene (33 Ma), and is related to the large scale sinistral slip-shearing since the Early Cenozoic.

ACKNOWLEDGMENTS

REFERENCES CITED

Aït-Djafer, S., Adjerid, Z., Badani, A., et al., 2009. Spinel-Quartz High Temperature Paragenesis in Al-Fe Granulites from the Ihouhaouene Area (NW Hoggar, Algeria). *Journal of African Earth Sciences*, 55(1/2): 79–91. https://doi.org/10.1016/j.jafrearsci.2009.02.004

Anderson, J. R., Payne, J. L., Kelsey, D. E., et al., 2012. High-Pressure Granulites at the Dawn of the Proterozoic. *Geology*, 40(5): 431–434. https://doi.org/10.1130/g32854.1

Bertrand, P., Ellis, D. J., Green, D. H., 1991. The Stability of Sapphirine-Quartz and Hypersthene-Sillimanite-Quartz Assemblages: An Experimental Investigation in the System FeO-MgO-Al$_2$O$_3$-SiO$_2$ under H$_2$O and CO$_2$ Conditions. *Contributions to Mineralogy and Petrology*, 108(1/2): 55–71. https://doi.org/10.1007/bf00307326

Brown, M., 2007. Metamorphic Conditions in Orogenic Belts: A Record of Secular Change. *International Geology Review*, 49(3): 193–234. https://doi.org/10.2747/0020-6814.49.3.193

Burchfiel, B. C., Wang, E., 2003. Northwest-Trending, Middle Cenozoic, Left-Lateral Faults in Southern Yunnan, China, and Their Tectonic Significance. *Journal of Structural Geology*, 25(5): 781–792. https://doi.org/10.1016/s0191-8141(02)00065-2

Bureau of Geology and Resources of Yunnan (BGMRY), 1990. Regional Geology of Yunnan. Geological Publishing House, Beijing. 1–290 (in Chinese)

Cao, S. Y., Liu, J. L., Leiss, L., et al., 2011a. Initiation of Left-Lateral Deformation along the Ailao Shan-Red River Shear Zone: New Microstructural, Textural, and Geochronological Constraints from the Diancang Shan Metamorphic Massif, SW Yunnan, China. *International Geology Review*, 54(3): 348–367. https://doi.org/10.1080/00206814.2010.543789

Cao, S. Y., Neubauer, F., Liu, J. L., et al., 2011b. Exhumation of the Diancang Shan Metamorphic Complex along the Ailao Shan-Red River Belt, Southwestern Yunnan, China: Evidence from ^{40}Ar/^{39}Ar Thermochronology. *Journal of Asian Earth Sciences*, 42(3): 525–550. https://doi.org/10.1016/j.jseaes.2011.04.017

Dong, Y. F., Zheng, C. Q., Zhou, X. W., et al., 2018. Metamorphism and Its Tectonic Implications of Early Mesozoic Pelitic Granulites from Badu Complex of Southwestern Zhejiang Province, South China. *Earth Science*, 43(1): 259–277 (in Chinese with English Abstract)

Dong, Y. P., Zhu, B. Q., Chang, X. Y., et al., 2000. Geochemistry of the Two-Type Volcanic Rocks from Ailaoshan Suture Zone and Their Tectonic Implication. *Geochimica*, 1: 1–13 (in Chinese with English Abstract)

Gilotti, J. A., Elvevold, S., 2002. Extensional Exhumation of a High-Pressure Granulite Terrane in Payer Land, Greenland Caledonides: Structural, Petrologic, and Geochronologic Evidence from Metapelites. *Canadian Journal of Earth Sciences*, 39(8): 1169–1187. https://doi.org/10.1139/e02-019

Harley, S. L., 2004. Extending Our Understanding of Ultrahigh Temperature Crustal Metamorphism. *Journal of Mineralogical and Petrological Sciences*, 99(4): 140–158. https://doi.org/10.2465/jmps.99.140

Harley, S. L., 2008. Refining the *P-T* Records of UHT Crustal Metamorphism. *Journal of Metamorphic Geology*, 26(2): 125–154. https://doi.org/10.1111/j.1525-1314.2008.00765.x

Hensen, B. J., Green, D. H., 1972. Experimental Study of the Stability of Cordierite and Garnet in Pelitic Compositions at High Pressures and Temperatures. *Contributions to Mineralogy and Petrology*, 35(4): 331–354. https://doi.org/10.1007/bf00371314

Hiroi, Y., Ogo, Y., Namba, K., 1994. Evidence for Prograde Metamorphic Evolution of Sri Lankan Pelitic Granulites, and Implications for the Development of Continental Crust. *Precambrian Research*, 66(1/2/3/4): 245–263. https://doi.org/10.1016/0301-9268(94)90053-1

Hiroi, Y., Shiraishi, K., Yanai, K., et al., 1983. Aluminum Silicates in the Prince Olav and Soya Coasts, East Antarctica. *Memoirs of National Institute of Polar Research, Special Issue*, 28: 115–131

Holdaway, M. J., 2000. Application of New Experimental and Garnet Margules Data to the Garnet-Biotite Geothermometer. *American Mineralogist*, 85(7/8): 881–892. https://doi.org/10.2138/am-2000-0701

Hu, Z. C., Liu, Y. S., Gao, S., et al., 2012. Improved *in situ* Hf Isotope Ratio Analysis of Zircon Using Newly Designed X Skimmer Cone and Jet Sample Cone in Combination with the Addition of Nitrogen by Laser Ablation Multiple Collector ICP-MS. *Journal of Analytical Atomic Spectrometry*, 27(9): 1391–1399. https://doi.org/10.1039/c2ja30078h

Jian, P., Liu, D. Y., Kröner, A., et al., 2009. Devonian to Permian Plate Tectonic Cycle of the Paleo-Tethys Orogen in Southwest China (I): Geochemistry of Ophiolites, Arc/Back-Arc Assemblages and Within-Plate Igneous Rocks. *Lithos*, 113(3/4): 748–766. https://doi.org/10.1016/j.lithos.2009.04.004

Jian, P., Liu, D. Y., Sun, X. M., 2008. SHRIMP Dating of the Permo–Carboniferous Jinshajiang Ophiolite, Southwestern China: Geochronological Constraints for the Evolution of Paleo-Tethys. *Journal of Asian Earth Sciences*, 32(5/6): 371–384. https://doi.org/10.1016/j.jseaes.2007.11.006

Jian, P., Wang, X. F., He, L. Q., et al., 1998. U-Pb Zircon Dating of the Shuanggou Ophiolite from Xingping County, Yunnan Province. *Acta Petrologica Sinica*, 14(2): 207–211 (in Chinese with English Abstract)

Jöns, N., Schenk, V., 2011. The Ultrahigh Temperature Granulites of Southern Madagascar in a Polymetamorphic Context: Implications for the Amalgamation of the Gondwana Supercontinent. *European Journal of Mineralogy*, 23(2): 127–156. https://doi.org/10.1127/0935-1221/2011/0023-2087

Koziol, A. M., Newton, R. C., 1988. Redetermination of the Anorthite Breakdown Reaction and Improvement of the Plagioclase-Garnet-Al$_2$SiO$_5$-Quartz Geobarometer. *American Mineralogist*, 73(3/4): 216–223. https://doi.org/10.1016/0370-2693(68)90152-4

Leloup, P. H., Kienast, J.-R., 1993. High-Temperature Metamorphism in a Major Strike-Slip Shear Zone: The Ailao Shan-Red River, People's Republic of China. *Earth and Planetary Science Letters*, 118(1/2/3/4): 213–234. https://doi.org/10.1016/0012-821x(93)90169-a

Leloup, P. H., Lacassin, R., Tapponnier, P., et al., 1995. The Ailao Shan-Red River Shear Zone (Yunnan, China), Tertiary Transform Boundary of Indochina. *Tectonophysics*, 251(1/2/3/4): 3–84. https://doi.org/10.1016/0040-1951(95)00070-4

Lepvrier, C., Maluski, H., Van Tich, V., et al., 2004. The Early Triassic Indosinian Orogeny in Vietnam (Truong Son Belt and Kontum Massif): Implications for the Geodynamic Evolution of Indochina. *Tectonophysics*, 393(1/2/3/4):

87–118. https://doi.org/10.1016/j.tecto.2004.07.030

Lepvrier, C., Maluski, H., Van Vuong, N., et al., 1997. Indosinian NW-Trending Shear Zones within the Truong Son Belt (Vietnam) ⁴⁰Ar-³⁹Ar Triassic Ages and Cretaceous to Cenozoic Overprints. *Tectonophysics*, 283(1/2/3/4): 105–127. https://doi.org/10.1016/s0040-1951(97)00151-0

Liang, H. Y., Campbell, I. H., Allen, C. M., et al., 2007. The Age of the Potassic Alkaline Igneous Rocks along the Ailao Shan-Red River Shear Zone: Implications for the Onset Age of Left-Lateral Shearing. *The Journal of Geology*, 115: 231–242. https://doi.org/10.1086/510801

Liu, F. T., Liu, J. H., Zhong, D. L., et al., 2000. The Subducted Slab of Yangtze Continental Block beneath the Tethyan Orogen in Western Yunnan. *Chinese Science Bulletin*, 45(5): 466–472. https://doi.org/10.1007/bf02884953

Liu, J. L., Cao, S. Y., Zai, Y. F., et al., 2007. Rotation of Crustal Blocks as an Explanation of Oligo–Miocene Extension in Southeastern Tibet—Evidenced by the Diancangshan and nearby Metamorphic Core Complexes. *Earth Science Frontiers*, 14(4): 40–48 (in Chinese with English Abstract)

Liu, J. L., Chen, X. Y., Wu, W. B., et al., 2015. New Tectono-Geochronological Constraints on Timing of Shearing along the Ailao Shan-Red River Shear Zone: Implications for Genesis of Ailao Shan Gold Mineralization. *Journal of Asian Earth Sciences*, 103: 70–86. https://doi.org/10.1016/j.jseaes.2014.11.006

Liu, J. L., Tang, Y., Tran, M. D., et al., 2012. The Nature of the Ailao Shan-Red River (ASRR) Shear Zone: Constraints from Structural, Microstructural and Fabric Analyses of Metamorphic Rocks from the Diancang Shan, Ailao Shan and Day Nui Con Voi Massifs. *Journal of Asian Earth Sciences*, 47: 231–251. https://doi.org/10.1016/j.jseaes.2011.10.020

Metcalfe, I., 2002. Permian Tectonic Framework and Palaeogeography of SE Asia. *Journal of Asian Earth Sciences*, 20(6): 551–566. https://doi.org/10.1016/s1367-9120(02)00022-6

Mo, X. X., Lu, F. X., Shen, S. Y., 1993. Sanjiang Tethyan Volcanism and Related Mineralization. Geological Publishing House, Beijing. 178–235 (in Chinese with English Abstract)

Morley, C. K., 2002. A Tectonic Model for the Tertiary Evolution of Strike-Slip Faults and Rift Basins in SE Asia. *Tectonophysics*, 347(4): 189–215. https://doi.org/10.1016/s0040-1951(02)00061-6

Morley, C. K., 2007. Variations in Late Cenozoic–Recent Strike-Slip and Oblique-Extensional Geometries, within Indochina: The Influence of Pre-Existing Fabrics. *Journal of Structural Geology*, 29(1): 36–58. https://doi.org/10.1016/j.jsg.2006.07.003

Motoyoshi, Y., Ishikawa, M., 1997. Metamorphic and Structural Evolution of Granulites from Rundvagshetta, Lützow-Holm Bay, East Antarctica. In: Ricci, C. A., ed., The Antarctic Region: Geological Evolution and Processes. Terra Antarctica, Sienna. 65–72

Motoyoshi, Y., Matsubara, S., Matsueda, H., 1989. *P-T* Evolution of the Granulite-Facies Rocks of the Lützow-Holm Bay Region, East Antarctica. *Geological Society, London, Special Publications*, 43(1): 325–329. https://doi.org/10.1144/gsl.sp.1989.043.01.26

Motoyoshi, Y., Matsubara, S., Matsueda, H., et al., 1985. Garnet-Sillimanite Gneisses from the Lützow-Holm Bay Region, East Antarctica. *Memoirs of National Institute of Polar Research, Special Issue*, 37: 82–94

Moulas, E., Kostopoulos, D., Connolly, J. A. D., et al., 2013. *P-T* Estimates and Timing of the Sapphirine-Bearing Metamorphic Overprint in Kyanite Eclogites from Central Rhodope, Northern Greece. *Petrology*, 21(5): 507–521. https://doi.org/10.1134/s0869591113050032

Nakano, N., Osanai, Y., Minh, N. T., et al., 2008. Discovery of High-Pressure Granulite-Facies Metamorphism in Northern Vietnam: Constraints on the Permo–Triassic Indochinese Continental Collision Tectonics. *Comptes Rendus Geoscience*, 340(2/3): 127–138.
https://doi.org/10.1016/j.crte.2007.10.013

Nakano, N., Osanai, Y., Owada, M., et al., 2004. Decompression Process of Mafic Granulite from Eclogite to Granulite Facies under Ultrahigh-Temperature Condition in the Kontum Massif, Central Vietnam. *Journal of Mineralogical and Petrological Sciences*, 99(4): 242–256. https://doi.org/10.2465/jmps.99.242

Nakano, N., Osanai, Y., Owada, M., et al., 2007. Geologic and Metamorphic Evolution of the Basement Complexes in the Kontum Massif, Central Vietnam. *Gondwana Research*, 12(4): 438–453. https://doi.org/10.1016/j.gr.2007.01.003

Nakano, N., Osanai, Y., Sajeev, K., et al., 2010. Triassic Eclogite from Northern Vietnam: Inferences and Geological Significance. *Journal of Metamorphic Geology*, 28(1): 59–76. https://doi.org/10.1111/j.1525-1314.2009.00853.x

Nam, T. N., Sano, Y., Terada, K., et al., 2001. First SHRIMP U-Pb Zircon Dating of Granulites from the Kontum Massif (Vietnam) and Tectonothermal Implications. *Journal of Asian Earth Sciences*, 19(1/2): 77–84. https://doi.org/10.1016/s1367-9120(00)00015-8

Nam, T. N., Toriumi, M., Itaya, T., 1998. *P-T-t* Paths and Post-Metamorphic Exhumation of the Day Nui Con Voi Shear Zone in Vietnam. *Tectonophysics*, 290(3/4): 299–318. https://doi.org/10.1016/s0040-1951(98)00054-7

O'Brien, P. J., Rötzler, J., 2003. High-Pressure Granulites: Formation, Recovery of Peak Conditions and Implications for Tectonics. *Journal of Metamorphic Geology*, 21(1): 3–20. https://doi.org/10.1046/j.1525-1314.2003.00420.x

Ogo, Y., Hiroi, Y., Prame, K., et al., 1992. A New Insight of Possible Correlation between the Lützow-Holm Bay Granulites (East Antarctica) and Sri Lankan Granulites. Recent Progress in Antarctic Earth Science. Terra Scientific Publishing Company, Tokyo. 75–86

Osanai, Y., Nakano, N., Owada, M., et al., 2004. Permo–Triassic Ultrahigh-Temperature Metamorphism in the Kontum Massif, Central Vietnam. *Journal of Mineralogical and Petrological Sciences*, 99(4): 225–241. https://doi.org/10.2465/jmps.99.225

Ouzegane, K., Boumaza, S., 1996. An Example of Ultrahigh-Temperature Metamorphism: Orthopyroxene-Sillimanite-Garnet, Sapphirine-Quartz and Spinel-Quartz Parageneses in Al-Mg Granulites from in Hihaou, in Ouzzal, Hoggar. *Journal of Metamorphic Geology*, 14(6): 693–708. https://doi.org/10.1111/j.1525-1314.1996.00049.x

Owada, M., Osanai, Y., Nakano, N., et al., 2007. Crustal Anatexis and Formation of Two Types of Granitic Magmas in the Kontum Massif, Central Vietnam: Implications for Magma Processes in Collision Zones. *Gondwana Research*, 12(4): 428–437. https://doi.org/10.1016/j.gr.2006.11.001

Pidgeon, R. T., 1992. Recrystallisation of Oscillatory Zoned Zircon: Some Geochronological and Petrological Implications. *Contributions to Mineralogy and Petrology*, 110(4): 463–472. https://doi.org/10.1007/bf00344081

Qi, X. X., Li, H. Q., Li, T. F., et al., 2010. Zircon SHRIMP U-Pb Dating for Garnet-Rich Granite Veins in High-Pressure Granulites from the Namche Barwa Complex, Eastern Syntaxis of the Himalayas, and the Relationship with Exhumation. *Acta Petrogica Sinica*, 26(3): 975–984 (in Chinese with English Abstract)

Qi, X. X., Santosh, M., Zhao, Y. H., et al., 2016. Mid-Neoproterozoic Ridge Subduction and Magmatic Evolution in the Northeastern Margin of the Indochina Block: Evidence from Geochronology and Geochemistry of Calc-Alkaline Plutons. *Lithos*, 248–251: 138–152. https://doi.org/10.1016/j.lithos.2015.12.028

Qi, X. X., Santosh, M., Zhu, L. H., et al., 2014. Mid-Neoproterozoic Arc Magmatism in the Northeastern Margin of the Indochina Block, SW China: Geochronological and Petrogenetic Constraints and Implications for Gondwana Assembly. *Precambrian Research*, 245: 207–224. https://doi.org/10.1016/j.precamres.2014.02.008

Qi, X. X., Zeng, L. S., Zhu, L. H., et al., 2012. Zircon U-Pb and Lu-Hf Isotopic Systematics of the Daping Plutonic Rocks: Implications for the Neoproterozoic Tectonic Evolution of the Northeastern Margin of the Indochina Block, Southwest China. *Gondwana Research*, 21(1): 180–193. https://doi.org/10.1016/j.gr.2011.06.004

Sano, Y., Terada, K., Hidaka, H., et al., 1999. Palaeoproterozoic Thermal Events Recorded in the ~4.0 Ga Acasta Gneiss, Canada: Evidence from SHRIMP U-Pb Dating of Apatite and Zircon. *Geochimica et Cosmochimica Acta*, 63(6): 899–905. https://doi.org/10.1016/s0016-7037(98)00303-2

Santosh, M., Tsunogae, T., Tsutsumi, Y., et al., 2009. Microstructurally Controlled Monazite Chronology of Ultrahigh-Temperature Granulites from Southern India: Implications for the Timing of Gondwana Assembly. *Island Arc*, 18(2): 248–265. https://doi.org/10.1111/j.1440-1738.2007.00601.x

Schaller, M., Steiner, O., Studer, I., et al., 1999. Exhumation of Limpopo Central Zone Granulites and Dextral Continent-Scale Transcurrent Movement at 2.0 Ga along the Palala Shear Zone, Northern Province, South Africa. *Precambrian Research*, 96(3/4): 263–288. https://doi.org/10.1016/s0301-9268(99)00015-7

Schärer, U., Tapponnier, P., Lacassin, R., et al., 1990. Intraplate Tectonics in Asia: A Precise Age for Large-Scale Miocene Movement along the Ailao Shan-Red River Shear Zone, China. *Earth and Planetary Science Letters*, 97(1/2): 65–77. https://doi.org/10.1016/0012-821x(90)90099-j

Searle, M. P., 2006. Role of the Red River Shear Zone, Yunnan and Vietnam, in the Continental Extrusion of SE Asia. *Journal of the Geological Society*, 163(6): 1025–1036. https://doi.org/10.1144/0016-76492005-144

Searle, M. P., Yeh, M.-W., Lin, T.-H., et al., 2010. Structural Constraints on the Timing of Left-Lateral Shear along the Red River Shear Zone in the Ailao Shan and Diancang Shan Ranges, Yunnan, SW China. *Geosphere*, 6(4): 316–338. https://doi.org/10.1130/ges00580.1

Sengör, A. C., 1984. The Cimmeride Orogenic System and the Tectonics of Eurasia. *Geological Society of America Special Paper*, 195: 82. https://doi.org/10.1130/spe195-p1

Tang, Y., Liu, J. L., Tran, M. D., et al., 2013. Timing of Left-Lateral Shearing along the Ailao Shan-Red River Shear Zone: Constraints from Zircon U-Pb Ages from Granitic Rocks in the Shear Zone along the Ailao Shan Range, Western Yunnan, China. *International Journal of Earth Sciences*, 102(3): 605–626. https://doi.org/10.1007/s00531-012-0831-y

Tapponnier, P., Lacassin, R., Leloup, P. H., et al., 1990. The Ailao Shan/Red River Metamorphic Belt: Tertiary Left-Lateral Shear between Indochina and South China. *Nature*, 343(6257): 431–437. https://doi.org/10.1038/343431a0

Tapponnier, P., Peltzer, G., Le Dain, A., et al., 1982. Propagating Extrusion Tectonics in Asia: New Insights from Simple Experiments with Plasticine. *Geology*, 10(12): 611–616. https://doi.org/10.1130/0091-7613(1982)10<611:petian>2.0.co;2

Trung, N. M., Tsujimori, T., Itaya, T., 2006. Honvang Serpentinite Body of the Song Ma Fault Zone, Northern Vietnam: A Remnant of Oceanic Lithosphere within the Indochina-South China Suture. *Gondwana Research*, 9(1/2): 225–230. https://doi.org/10.1016/j.gr.2005.06.012

Tsunogae, T., Santosh, M., 2006. Spinel-Sapphirine-Quartz Bearing Composite Inclusion within Garnet from an Ultrahigh-Temperature Pelitic Granulite: Implications for Metamorphic History and *P-T* Path. *Lithos*, 92(3/4): 524–536. https://doi.org/10.1016/j.lithos.2006.03.060

Wang, B. D., Wang, L. Q., Wang, D. B., et al., 2018. Tectonic Evolution of the Changning-Menglian Proto-Paleo Tethys Ocean in the Sanjiang Area, Southwestern China. *Earth Science*, 43(8): 2527–2550 (in Chinese with English Abstract)

Wang, J. H., Yin, A., Harrison, T. M., et al., 2001. A Tectonic Model for Cenozoic Igneous Activities in the Eastern Indo-Asian Collision Zone. *Earth and Planetary Science Letters*, 188(1/2): 123–133. https://doi.org/10.1016/s0012-821x(01)00315-6

Wang, X. F., Metcalfe, I., Jian, P., et al., 2000. The Jinshajiang-Ailaoshan Suture Zone, China: Tectonostratigraphy, Age and Evolution. *Journal of Asian Earth Sciences*, 18(6): 675–690. https://doi.org/10.1016/s1367-9120(00)00039-0

Wu, C. M., 2018. Metapelitic Garnet-Muscovite-Al$_2$SiO$_5$-Quartz (GMAQ) Geothermobarometry. *Journal of Earth Science*, 29(5): 977–988. https://doi.org/10.1007/s12583-018-0851-z

Wu, C. M., Zhang, J., Ren, L. D., 2004. Empirical Garnet-Biotite-Plagioclase-Quartz (GBPQ) Geobarometry in Medium- to High-Grade Metapelites. *Journal of Petrology*, 45(9): 1907–1921. https://doi.org/10.1093/petrology/egh038

Wu, W. B., Liu, J. L., Zhang, L. S., et al., 2017. Characterizing a Middle to Upper Crustal Shear Zone: Microstructures, Quartz *c*-Axis Fabrics, Deformation Temperatures and Flow Vorticity Analysis of the Northern Ailao Shan-Red River Shear Zone, China. *Journal of Asian Earth Sciences*, 139: 95–114. https://doi.org/10.1016/j.jseaes.2016.12.026

Yeh, M. W., Lee, T. Y., Lo, C. H., et al., 2008. Structural Evolution of the Day Nui Con Voi Metamorphic Complex: Implications on the Development of the Red River Shear Zone, Northern Vietnam. *Journal of Structural Geology*, 30(12): 1540–1553. https://doi.org/10.1016/j.jsg.2008.08.007

Yumul, G. P. Jr., Zhou, M. F., Wang, C. Y., et al., 2008. Geology and Geochemistry of the Shuanggou Ophiolite (Ailao Shan Ophiolitic Belt), Yunnan Province, SW China: Evidence for a Slow-Spreading Oceanic Basin Origin. *Journal of Asian Earth Sciences*, 32(5/6): 385–395. https://doi.org/10.1016/j.jseaes.2007.11.007

Zhang, J. J., Zhong, D. L., San, H. Q., et al., 2006. Structural and Geochronological Evidence for Multiple Episodes of Deformation since Paleocene along the Ailaoshan-Red River Shear Zone, Southeastern Asia. *Chinese Journal of Geology*, 41(2): 291–310 (in Chinese with English Abstract)

Zhang, J. J., Zhong, D. L., Zhou, Y., 1999. Tectonic Evolution of Southeast Asia and the Ailaoshan-Honghe Tectonic Belt. *Geological Review*, 45(4): 337–344 (in Chinese with English Abstract)

Zhang, J. X., Meng, F. C., 2005. Sapphirine-Bearing High Pressure Mafic Granulite and Its Implications in the South Altyn Tagh. *Chinese Science Bulletin*, 50(3): 265–269. https://doi.org/10.1007/bf02897537

Zhang, Q., Zhou, D. J., Li, X. Y., et al., 1995. Characteristics and Genesis of Shuanggou Ophiolites, Yunnan Provience, *China. Acta Petrologica Sinica*, 11(Suppl.): 190–202 (in Chinese with English Abstract)

Zhang, Q., Zhou, D. J., Zhao, D. S., et al., 1994. Ophiolites of the Hengduan Mountains, China: Characteristics and Tectonic Settings. *Journal of Southeast Asian Earth Sciences*, 9(4): 335–344. https://doi.org/10.1016/0743-9547(94)90044-2

Zhang, Z. M., Ding, H. X., Dong, X., et al., 2018. High-Temperature Metamorphism, Anataxis and Tectonic Evolution of a Mafic Granulite from the Eastern Himalayan Orogen. *Journal of Earth Science*, 29(5): 1010–1025. https://doi.org/10.1007/s12583-018-0852-y

Zhang, Z. M., Xu, Z. Q., Xu, H. F., 2000. Petrology of Ultrahigh-Pressure Eclogites from the ZK703 Drillhole in the Donghai, Eastern China. *Lithos*, 52(1/2/3/4): 35–50. https://doi.org/10.1016/s0024-4937(99)00083-3